Journal of Manufacturing Systems 63 (2022) 524–538

Contents lists available at ScienceDirect

Journal of Manufacturing Systems

journal homepage: www.elsevier.com/locate/jmansys

Effect of coaxial nozzle wear on catchment efficiency in direct energy deposition built components

Lisa DeWitte [a], Christopher Saldana [a], Thomas Kurfess [b], Katherine Fu [a,*]

[a] George W. Woodruff School of Mechanical Engineering, 801 Ferst Drive, Atlanta 30332, GA, USA
[b] Oak Ridge National Laboratory Manufacturing Demonstration Facility, 2370 Cherahala Blvd NTRC-2, Knoxville 37932, TN, USA

ARTICLE INFO

Keywords:
Catchment efficiency
Directed energy deposition
Hybrid manufacturing
Zero defect manufacturing
2000 MSC:
0000
1111
PACS:
0000
1111

ABSTRACT

Laser based Direct Energy Deposition (DED) systems using metallic powder feedstock are recognized as a promising manufacturing method for their ability to shorten production cycles and create complex part geometries. Components are built by generating a melt pool with a high-power laser beam while material is coaxially injected and left to solidify. An impediment to large scale use of DED lies in poor powder catchment efficiency, the condition in which a portion of injected powder escapes the melt pool resulting in a ratio of decreased printed material mass to mass of supplied feedstock. The wear state of a coaxial nozzle on a DED system within a hybrid manufacturing machine tool has been observed to decrease catchment efficiency over time. This study investigates this effect by adapting flow visualization techniques to an in-situ process monitoring format, the implementation of a Computational Fluid Dynamics (CFD) simulation, and deposition testing. Nozzle geometric defects due to wear are identified and categorized, and the impact of nozzle tip wear, resulting in axial tip reduction, on powder catchment efficiency is proven by multiple calculation methods. A linear correlation between catchment efficiency and powder stream diameter is identified, causing a 15–20% loss in efficiency sustained over incremental nozzle tip reduction up to − 1 mm. These results provide a foundation for further study of wear effects and Zero defect manufacturing solutions for powder fed DED systems.

1. Introduction

Laser based Directed Energy Deposition (DED) is an additive manufacturing (AM) process in which a high-powered laser melts feedstock to form a deposited bead, fed by a controlled stream of stock. This process creates a metallurgical bond between layers that is fused to the deposition surface, which is either the substrate or previously deposited layers [1]. Powder DED is utilized for small to medium sized parts that require minimal post processing due to the material deposition rates available, and the achievable surface finish [2,3]. Feedstock material is typically supplied via a gravitational feeder and inert carrier gas through the processing head, depositing powder coaxially or off axis into the melt pool [4,5].

Deposition heads equipped with coaxial nozzle assemblies deliver powder annularly, with the exiting powder descending in a cone shaped multi-phase flow to intersect with a centered laser beam [6]. Analyzing the design evolution of coaxial deposition over the last 30 years, these heads are typically composed of three individual nesting nozzles made from a material with high reflectivity and thermal conductivity, such as copper or brass. The inner nozzle in which the laser passes through and a jet of inert shield gas to protect laser components from particulate matter, the middle coaxial nozzle which provides the outer wall boundary for the powder and carrier gas flow, and the outer nozzle which also jettisons shield gas to prevent the deposition from oxidizing [7–10–13,14,15]. In any powder fed DED systems, disruption in the material mass flow rate has the potential to cause a corresponding surface irregularity in the deposited bead, making continuous uniform powder supply vital to high quality deposition [1]. Metal powder has a large range of material availability but suffers poor rates of material catchment. The escaped powder poses a health and environmental hazard if not properly disposed of, and is one of powder DED's least researched sustainability concerns [16–19,20].

The largest obstacles to industry wide adoption of AM include the inability to produce homogeneous finished surfaces, the presence of internal defects due to the deposition process, and the dimensional inaccuracy of as-built parts [7,21,22]. In powder-fed laser DED systems, specifically coaxially fed systems, the extent to which these disadvantages manifest relies heavily on a machine's powder catchment

* Corresponding author.
E-mail address: katherine.fu@gatech.edu (K. Fu).

https://doi.org/10.1016/j.jmsy.2022.05.004
Received 19 September 2021; Received in revised form 28 April 2022; Accepted 5 May 2022
Available online 21 May 2022

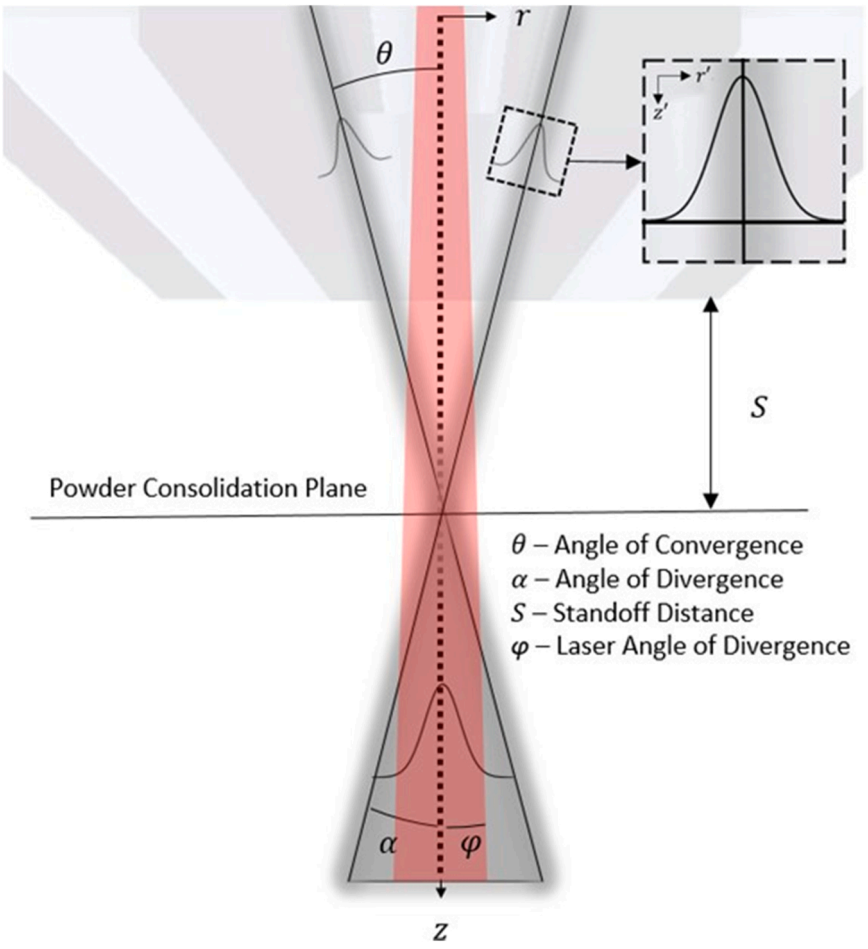

Fig. 1. Diagram of powder stream geometry, including the powder stream distribution pre-consolidation (inset) [40].

efficiency. It is beneficial to optimize the dimensions of the impacting powder stream, as altering the laser spot size will ultimately change the geometry of the deposited bead [23]. It is a common strategy to control powder stream geometry through various deposition process parameters [24,25]. Due to the constant subjection to heat and impacting powder, the middle nozzle tip in a coaxial AM head will wear down over time, creating an annular flow exit of increasing area. The resulting distortion to the powder flow eventually creates enough loss in catchment to warrant a replacement. As this nozzle is a consumable component and its frequent replacement adds cost to the manufacturing process, there is an incentive to optimize the life cycle of this consumable [18].

A wealth of research demonstrates both experimental and numerical powder flow measurement and visualization methods, however the research subject is usually coaxial nozzle design validation. One such example is an earlier coaxial nozzle designed for laser cladding by Lin et al., which achieved 40% powder catchment efficiency through use of a mathematical model, light sheet imaging https://www.overleaf.com/project/60fd99f20ae6964ea253cea6, a scanning powder sensor, and a two dimensional axisymmetric fluent model [4]. Likewise, Takemura et al. iteratively designed a coaxial nozzle using a computational fluid dynamics (CFD) simulation, the light sheet method, and deposition tests, demonstrating a catchment efficiency improvement from 50.2% to 66% in experimental results [26]. There exists a gap in the current body of literature of coaxial nozzle wear and performance throughout the consumable's lifecycle. By applying these methods demonstrated in coaxial nozzle design and analyzing the extent to which nozzle wear effects catchment efficiency, the point at which nozzle replacement is necessary can be identified. Furthermore, by adapting the experimental techniques used to determine this effect to an in-process monitoring format, it is possible to establish relationships between consumable wear and machine work hours so that the economic and print quality consequences of this consumable's timely replacement can be optimized through predictive maintenance.

The presented study of this wear is conducted within a hybrid machine tool with five axis milling capabilities. Advances in AM, specifically since incorporation into hybrid manufacturing machine tools, often bear similarity to established methods of subtractive manufacturing (SM). This can be seen in the recent industry push for in-situ process monitoring, cyberphysical systems, and closed loop feedback control through the Industry 4.0 movement[27–29]. These elements have already been implemented widely in machining applications, contributing to next generation process quality control concepts such as Zero Defect Manufacturing (ZDM) [30,31]. A product-specific example is the development of individualized specialty AM processing heads for specific cladding processes that are able to be easily swapped in and out of a host AM or hybrid unit, not unlike tool changing capabilities exhibited by CNC machining cells [32–34]. Likewise, the motivation of this study is to optimize AM performance by accounting for wear in replaceable components, not unlike accounting for tool wear in the production of machined parts.

The middle coaxial nozzle in a standard powder fed laser DED head assembly is a regularly replaced consumable. Its state of wear has been observed to affect print quality over time as the nozzle tip deteriorates, yet no knowledge on quantifying this effect currently exists. The objective of this research is to establish the relationship between middle coaxial nozzle wear and print quality by measuring the nozzle's catchment efficiency. If the experimental methods are adapted into an in-situ monitoring format, this effect can be routinely monitored and accounted

for by adjusting process parameters. Quality improvement process changes that occur before the start of a DED deposition, or process changes that are predictive in nature, can be achieved by leveraging the detection capabilities of an in-situ flow visualization apparatus with the level of prognostic analysis achievable using CFD simulations to create a digital twin of a manufacturing process [30,31].

2. Theory and calculations

2.1. Powder stream geometry

Early analytical models of coaxial powder streams approximated powder flow as a cylinder of constant width. This was improved upon by Lin, identifying three critical powder flow regions: a converging annular stream immediately past the nozzle exit, the plane of convergence in which the powder is most focused, and an expanding stream post-convergence bearing a circular cross-sectional profile with a near Gaussian distribution. It was also confirmed experimentally that a post-convergence powder stream concentration had a Gaussian distribution, and that inner and shield gas flows affect the powder stream spraying angle [7,35,36].

This analytical model was further expanded by Pinkerton and Lin to account for the inclination angle of the tapered annular stream and to directly associate gas flow rates and coaxial nozzle geometry. The same three powder stream regions were identified, and separate coordinate systems were used above and below the plane of powder consolidation [37–39]. A diagram of the independently derived model used to characterize experimental image data is provided in Fig. 1.

In this work, the deposition laser as well as the concentrations of both the annular stream and converged stream regions were assumed to have a Gaussian profile, and the corresponding expression for the powder concentration profile was integrated about the central axis. The two different coordinate systems are used to describe powder flow geometry above and below the plane of convergence. The coordinate system (r', z') describes the orientation of the unmerged annular powder stream with the origin set at the nozzle outlet annulus, and the coordinate system (r, z) describes the orientation of the merged powder stream. In regard to the second coordinate system, z corresponds to the central axis of the nozzle assembly and the origin is placed at the intersection of the central axis and the nozzle exit plane. Serving as a link between these coordinate systems, the point location of this plane is denoted as z' and z_P in Eqs. (1) and (2). In addition, the r' and z' coordinate transformation is described in Eqs. (3) and (4), respectively.

$$z' = \frac{(r_i + r_o)}{2\sin\theta} \tag{1}$$

$$z' = \frac{(r_i + r_o)}{2\tan\theta} \tag{2}$$

$$r' = z\sin\theta + r\cos\theta - \frac{1}{2}(r_i + r_o)\cos\theta \tag{3}$$

$$z' = z\cos\theta + r\sin\theta \tag{4}$$

In these equations, r_i and r_o represent the inner and outer annular radius of the mid-coaxial nozzle, and θ denotes the powder stream angle of convergence. Setting stream width limits at $1/e^2$, which defines the stream edge at 2σ, the powder flow concentration C between the nozzle exit and before any occurrence of merging powder streams $(0 \le z' \le z')$ is defined in Eq. (5). Mass flow rate is represented as m', and Q indicates volumetric flow rate.

$$C(r') = \frac{2m'}{Q\sqrt{\pi}erf[1]} e^{\frac{-2(r_i + r_o - 2r - 2z\tan\theta)^2}{(r_o - r_i)^2}} \tag{5}$$

The concentration immediately before the plane of convergence exhibits the convergence of two streams as described in the following equation, taking note that $r \to 0$ as z approaches the central axis. After that, Eq. (2) is substituted in as z to evaluate concentration at the plane of convergence in Eq. (6).

$$C(r, z) = \frac{4m'}{Qvperf[1]} e^{\frac{-8r'^2}{(r_o - r_i)^2 \cos^2\theta}} \tag{6}$$

For the fully merged and expanding powder flow, $z > z_P$ and the equation for powder flow concentration further reduces into Eqs. (7) and (8) for stream diameter D, and maximum concentration C^* which occurs along the central axis at $r = 0$.

$$D = \frac{2(r_o - r_i)z\tan\theta}{(r_i + r_o)} \tag{7}$$

$$C*(0, z) = \frac{2(r_i + r_o)m'}{Qerf[1]z\tan\theta} \tag{8}$$

2.2. Coaxial nozzle performance

It can be seen that the most advantageous placement of substrate, and by extension the melt pool, would occur after the plane of convergence in which flow stream diameter is governed by Eq. (6) and peak concentrations of both powder and laser energy density occur along the central axis. Furthermore, the location of this plane is related to the convergent powder spraying angle, which is in turn controlled by the flow velocities of the inner, carrier, and shield gas jets [4]. Eq. (9) utilizes the property of Gaussian distribution displayed by the powder stream in calculating the diametric ratio between the Gaussian distributed laser diameter d_g and the full Gaussian distributed powder stream diameter D_g:

$$\eta = \frac{d_g}{D_g} = \frac{erf\left(\frac{d}{\sqrt{2}}\right)}{erf\left(\frac{D}{\sqrt{2}}\right)} \tag{9}$$

This expression indicates that either a decrease in powder stream diameter or an increase in laser beam diameter is an efficient way to improve powder catchment [36].

2.3. Powder stream numerical simulation

While appropriate for approximation and process parameter development, the practical limits of analytical models necessitate numerical simulations, which typically employ computational fluid dynamics (CFD) [41,37,42–45]. The Navier Stokes system of differential equations establishes the mathematical basis for this numerical model, with the fluid carrier gas and solid powder particle injection modeled as a coupled two-phase turbulent flow. While all gas flows are modeled continuously, a discrete phase model (DPM) is used to represent the injected powder particles and their trajectories. Since the experimental conditions that the simulation is intended to represent do not require the use of laser power, the gas flow is assumed to be isothermal and the thermal energy contributions of any gas-powder interactions are assumed to be negligible. Powder particle diameter is presented as a Rosin-Rammler distribution across a specified range [46,47]. The presence of turbulent flows is approximated with a realizable $k - \epsilon$ model.

2.4. Powder stream monitoring

Improvement in powder DED catchment efficiency depends on the monitoring and control of both laser and powder stream dimensions [21]. While in-process monitoring is well integrated in industrial applications for subtractive processes, such infrastructure remains in its infancy for AM processes [48]. For laser based DED, most in-situ monitoring methods exist for the purpose of predicting the thermal profile and material quality of the deposition. These include the use of various instruments such as a pyrometer or infrared (IR) camera [49–52,

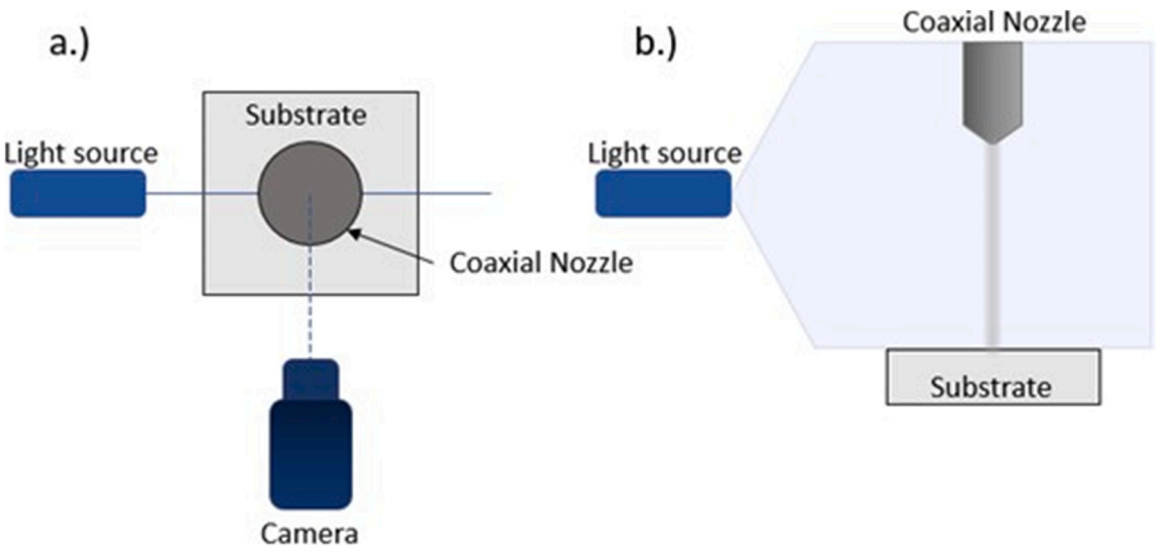

Fig. 2. a) Top view and b) Camera view of an axial light sheet imaging setup.

53,54]. Flow visualization methods and image analysis have been consistently used in coaxial powder systems to validate designs, analytical, and numerical models yet have little to no in-process counterpart [26,55–58,59,60]. As such there are limited means of accurately monitoring powder stream geometry to institute process control or predictive maintenance timelines [48].

Light sheet imaging is a well-established and popular flow visualization technique and produces a two-dimensional cross section of a laser based DED powder stream. This involves placing a collimated beam behind either a slit mask or cylindrical lens, creating a planar sheet of light that can be positioned either axially or transversely in the powder stream while the deposition laser is not engaged. A digital camera is positioned either normal to the light sheet or at a known location to capture the attenuated light scattered by powder particles, as seen in Fig. 2. Luminosity in the resulting captured images can be assumed to be directly proportional to mid-stream powder concentrations. This relationship is based on single scattering conditions specified by Mie's theory of the scattering of light by small particles [41,61,40].

3. Materials and methods

3.1. Equipment

All powder imaging and deposition experiments were performed within the enclosure of the Mazak VC500 AM, a multitasking hybrid machine tool based on the VCU, a series of 5-axis CNC mills. In addition to CNC machining capabilities, this system is retrofitted with a powder feed system, laser unit, and a DED head. While the deposition head is located inside the machine enclosure, the powder feeder and deposition laser units are housed externally on the side. The trunnion style spindle column houses the deposition head, laser optics, as well as the powder and gas delivery subsystem, in addition to being responsible for translational movement in three axes. The work holding table is able to be rotated in two axes as well. All motion is controlled with G-code commands interpreted by the machine controller. Movement command of the deposition head is achieved by specification of a secondary "spindle" axis horizontally offset from the original, effectively shifting the trunnion coordinate system in the positive x-direction [62]. The machine enclosure is spacious enough to house and accommodate in-process monitoring systems used to assess machine performance.

The spindle column mounted deposition head is produced by Hybrid Manufacturing Technologies and the nozzle configuration used is most similar to the S3 Sidemount System, model 3935. The deposition head is

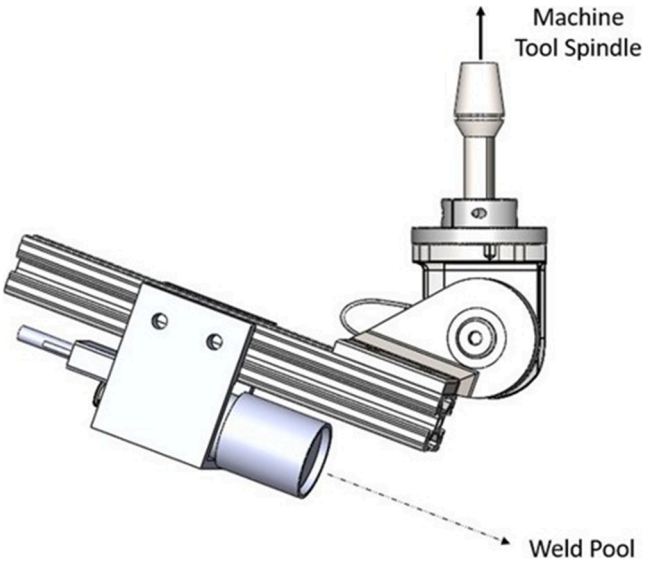

Fig. 3. Adjustable spindle clamped camera mount.

also capable of independent movement up and down the secondary, offset z-axis to the spindle, but is still coupled to the XYZ translation of the milling spindle.

An Oerlikon Twin-150 powder feeder is used to regulate flow by specifying a duty cycle percentage through controller commands. Properly calibrated, this multipurpose feeder dispenses a directly proportionate mass amount of powder, which is fed from a 5.0 L hopper through to the deposition head using argon as a carrier gas. A pressure regulator attached to the inlet gas flow ensures that carrier, inner, and shield gas is released at a gauge pressure of 0.3 MPa.

As the milling spindle is not in use during AM operations, a spindle clamped digital camera mount was constructed to record close up image data of powder flow and depositions. Given the spacious machine enclosure, appropriate work offsets and relatively low thermal dispersion of powder fed DED systems, the camera is able to capture images of the nozzle and melt pool area in a configuration normal to the YZ plane facing the deposition head without incurring damage due to heat or collisions, illustrated in Fig. 3. A Basler acA800–200gc area scan camera was used for image collection, with image acquisition settings controlled by its accompanying software on a desktop computer. A self-leveling

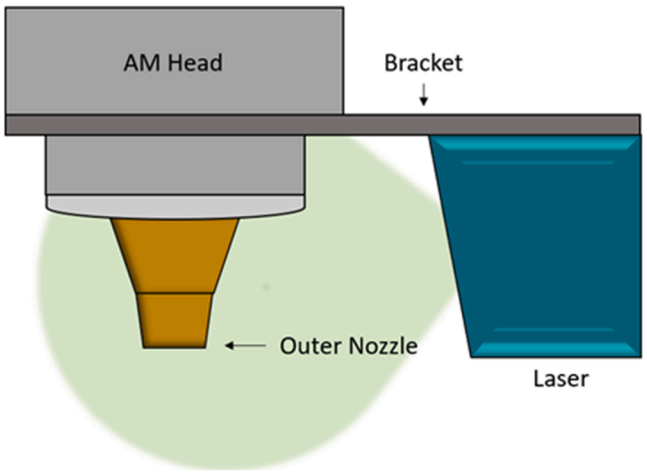

Fig. 4. An in-process setup for light sheet imaging.

Class 2 line laser was positioned normal to the XZ plane facing the deposition head and bisecting the middle of the outflowing powder stream. This was achieved through the construction of a modified security camera wall mount bracketed to the spindle column.

3.2. Light sheet imaging

The equipment configuration seen in Fig. 4 used to image the powder was housed inside the VC500AM machining enclosure, which limited ambient light from affecting captured data. In addition, a datum image was collected before beginning any trial and was subtracted from experimental images as a part of image processing. Lastly, to justify omission of multiple scattering effects, luminosity values were collected from a 20 by 20-pixel test region of powder streams produced by different powder feeder duty cycles ranging from 10% to 90% in 5% increments. Pixel luminosity is quantified by its gray value, ranging from 0 to 255 for an 8-bit image. The resulting linear trend observed in Fig. 5 indicates a direct proportionality between powder concentration and powder luminance [41,62].

Powder flow from all tested coaxial nozzles were imaged cold to establish basic shape and wear influence independent of thermal gradients. Experiments were conducted using a parameter set used in past low risk deposition processes on the VC500AM as described in Table 1. Powder mass flow rate, the last listed item in Table 1, was obtained by discharging powder into a tared cup of water for two minutes and measuring the difference in mass [63,64]. This preliminary test was repeated for 10 trials to produce an averaged value. The scattered laser light from powder particles was recorded, then processed with a MATLAB script that converted all images to grayscale, averaged ten collected frames together, subtracted the gray values of the datum image, and applied a Gaussian low pass filter for smoothness.

Qualitative analysis was performed with nozzles previously used in production (Fig. 6) to observe powder stream behavior, determine possible impacts wear geometry had on powder flow, and identify key regions of interest discussed in literature: a converging region, the plane of stream convergence at which the powder stream diameter is smallest, and a diverging powder stream [60]. To isolate and observe the specific effects of coaxial nozzle tip wear, a set of coaxial nozzles were machined with identical inner profiles to the manufacturer sourced coaxial nozzles and fabricated wear surfaces. Pixel luminance values collected from these nozzles were used as a comparison data set to study the distribution of calculated powder concentration values obtained by CFD simulation at several standoff distances, including the standoff distance later used for deposition. All collected images to be used in powder stream geometry analysis were cropped to a region of interest equivalent to 5 mm standoff distance from the tip of a new nozzle. All reported standoff distances indicate the axial distance from a new nozzle tip, regardless of the nozzle wear state being tested, as this dimension is shared with the outer nozzle tip as well. The tip of the outer nozzle (and a new, unworn mid-coaxial nozzle) is considered the actual exit plane of the AM head, even though powder stream expansion is possible before this point due to mid-coaxial nozzle wear.

Table 1
Light sheet imaging machine operating parameters.

Parameter	Operating value (Unit)	Description
Inner Gas Flow Rate	2 (L/min)	Gas flow to preserve laser lens quality
Carrier Gas Flow Rate	6 (L/min)	Gas flow delivering powder
Shield Gas Flow Rate	6 (L/min)	Gas flow protecting melt pool area
Powder Feeder Duty Cycle	35 (%)	Signal corresponding to a volumetric measurement of powder
Powder Mass Flow Rate	2.535 ± 3.670E-2 (g/min)	Corresponding mass flow rate of powder at 35% DC

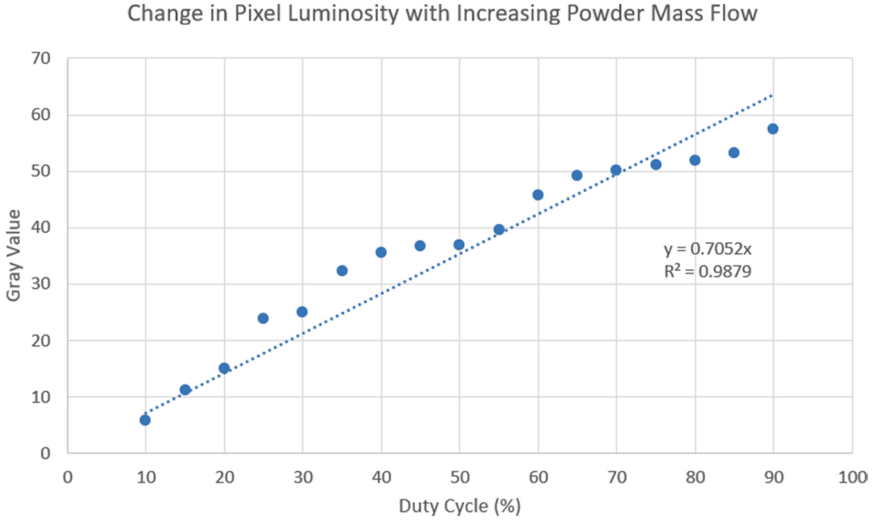

Fig. 5. Linear relationship between powder feeder duty cycle and pixel luminosity.

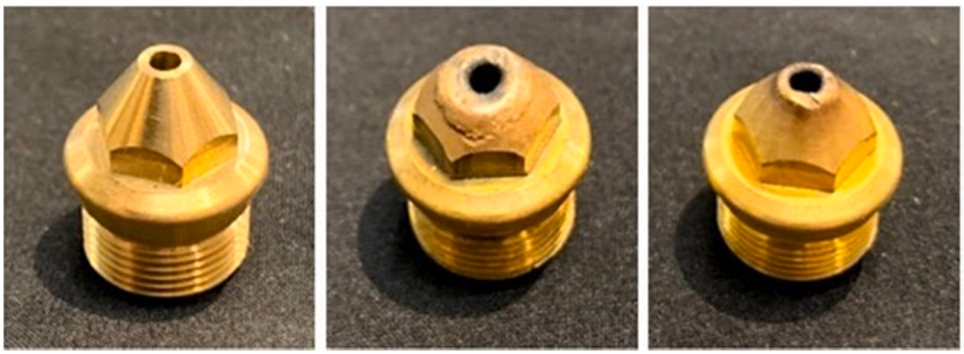

Fig. 6. Observed geometric irregularities (center and right) in contrast to an unworn mid-coaxial nozzle (left).

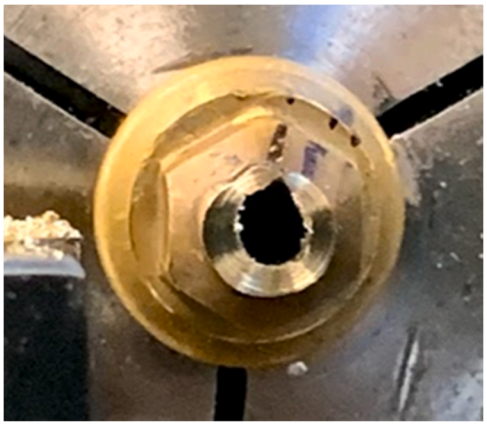

Fig. 7. Example of interior nozzle wear.

3.3. Characterizing and fabricating nozzle wear

Nozzle wear characterization began with examination and powder flow imaging of mid-coaxial nozzles retired from machine use at various states of wear and comparing them to the appearance and performance of a manufacturer supplied nozzle never used in deposition. Two geometric irregularities related to tip wear were a jagged, uneven nozzle tip and a smooth region extending from the tip edge to the nozzle outer contour. The collected images of powder flow geometry for each nozzle were analyzed to determine the presence of powder stream convergence and divergence at $\pm 2\sigma$ and $\pm \sigma$ intervals (95.4% and 68.2% of injected powder respectively). The presence of a completely divergent stream was noted as an example of critical performance failure. In an effort to isolate other sources of wear inducing erratic powder flow geometry, a series of mid-coaxial nozzles were designed with final dimensions varying in tip deterioration. Initial attempts to manufacture these nozzles with fabricated wear geometry involved resurfacing the tips of retired mid-coaxial nozzles, but additional eroded regions were discovered on the nozzle's inner taper. Observable in Fig. 7, these regions altered the radial symmetry of the interior contour as well.

As a result, replicant nozzles were manufactured to isolate the effects of nozzle tip deterioration resulting in a reduction on the axial dimension. The dimensions and material of the mid-coaxial nozzle were obtained by reverse engineering, and the replicant nozzles fabricated out of 360 machinable brass using an Okuma Genos L250 2 axis CNC lathe. The internal taper of the resulting replicant nozzles was within $\pm$ 0.05° that of the original nozzle, while on the external profile, a few superficial features were omitted for toolpath planning purposes. These differences can be observed in Fig. 8. Five trials were manufactured: one control case that did not have any recreated tip wear, and four trials with tip wear in the amounts of $-$ 0.25 mm, $-$ 0.50 mm, $-$ 0.75 mm, and $-$ 1.00 mm. As in the initial mid-coaxial nozzle characterization, powder flow similarity of the replicant nozzle to the original nozzle was assessed by comparing the control (unworn) trials of each using the same light sheet image collection and analysis used in the assessment of experimental nozzle geometries.

3.4. CFD simulation

Powder and gas flow through the coaxial AM head assembly was

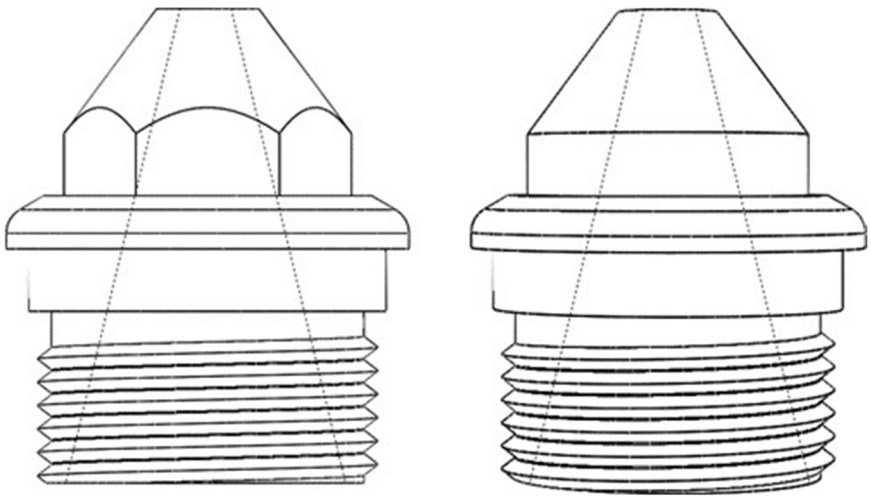

Fig. 8. Drawing of original (left) and fabricated (right) nozzle.

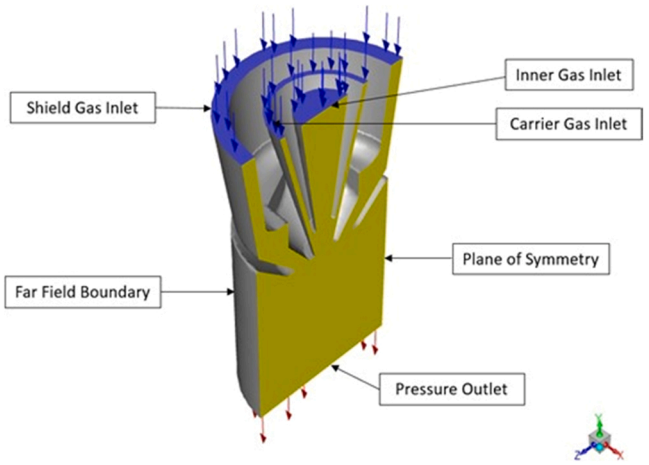

Fig. 9. Flow field geometry and locations of important boundary conditions.

Table 2
Inlet/outlet boundary conditions.

Boundary plane	Boundary condition	Velocity (m/s)	Gage pressure (Pa)	DPM BC
Carrier Gas Inlet	Velocity Inlet	6.7591	3E5	escape
Inner Gas Inlet	Velocity Inlet	4.9602E-1	3E5	escape
Shield Gas Inlet	Velocity Inlet	4.9855	3E5	escape
Plane of Symmetry	Symmetrical	–	–	reflect
Nozzle Walls	No Slip, Enhanced Wall Treatment	–	–	reflect
Far Field Region	No Slip, Enhanced Wall Treatment	–	–	escape
Gas Flow Outlet	Pressure Outlet	–	0	escape

Table 3
Physical properties and constants.

Symbol	Value (Unit)	Description
ρ_s	8000 (kg/m^3)	Density of 316SS
ρ_a	1.225 (kg/m^3)	Density of argon gas
g	9.81 (m/s^2)	Gravitational constant
μ	1.789E-5 (kg/m · s)	Viscosity
μ_t	1	Turbulent viscosity
C^2	1.9	Constant used in the ϵ transport equation
σ_κ	1	Turbulent kinetic energy Prandtl Number
σ_ϵ	1	Turbulent dissipation rate Prandtl Number
κ	0.8	Turbulent kinetic energy
ϵ	0.8	Turbulent viscosity

completed using ANSYS Workbench 2020 R1. Flow field geometry was reverse engineered and recreated using a polyhedral mesh and an assumption of symmetrical flow, resulting in quicker computation times that allow for timely changes when modeling future process parameter settings and illustrated in Fig. 9. Separate simulations were run for each instance of manufactured nozzle wear, each with its fluid flow geometry reflecting the wear state dimensions.

A pressure-based solver was used to establish a steady state model, with inlet velocity values approximated from the operating parameters in Table 1 using volumetric flow ratios. While argon gas was continuously modeled, AISI 316 L Stainless Steel (SS) powder particles were represented by a DPM, and both phases were free to interact with each other.

Argon gas was released from three concentric velocity inlet faces

Table 4
Rosin-rammler parameters.

Parameter	Value
Min. Diameter	6e-8 m
Max. Diameter	1.2e-7 m
Mean. Diameter	7.5e-8 m
Spread Parameter	3.5
Number of Diameters	20

Table 5
Machine operating parameters during deposition.

Parameter	Operating value (Unit)	Description
Inner Gas Flow Rate	2 (L/min)	Gas flow to preserve laser lens quality
Carrier Gas Flow Rate	6 (L/min)	Gas flow delivering powder
Shield Gas Flow Rate	6 (L/min)	Gas flow protecting melt pool area
Powder Feeder Duty Cycle	35 (%))	Signal corresponding to a volumetric measurement of powder
Powder Mass Flow Rate	2.535 ± 3.67E-2 (g/min)	Corresponding flow rate of powder feeder at 35% DC
Laser Power	350(W)	Laser energy output
Laser Spot Size Diameter	1 (mm)	Diameter of the deposition laser at 1/e^2 width (or ± 2σ)
C^2	1.9	Constant used in the ϵ transport equation
C^2	1.9	Constant used in the ϵ transport equation
Clad Speed	300 (mm/min)	Traveling speed of the additive head
Programmed Clad Length	12.5 (mm)	Length specified in machine code commands

(inner, carrier, and shield), while a Rosin-Rammler distribution of powder particles were released normal to the planar surface of the carrier velocity inlet. Powder diameters used as Rosin-Rammler parameters were obtained from a powder size distribution study used in past work and conducted on the same AISI 316 L SS powder, which was procured from Carpenter Additive [64]. The particle mass flow rate, 2.1961E-5 kg/s, was approximated from the mass flow rate of the powder feeder at 35% DC. Turbulent particle dispersion was governed by a discrete random walk model and spherical drag law (17). Boundary conditions, constant values and other parameters are listed in Tables 2–4. The geometry of the resultant simulated powder flow was ascertained by particle tracking and probing for traverse profiles of particle mass concentration (reported in units of kg^*m^3) at various standoff distances including the deposition standoff of 2.75 mm.

3.5. Deposition experiment

Five single bead lines were deposited for each test nozzle on 316 L SS substrate, 12.5 mm in length. Relevant print process parameters were consistent with light sheet imaging parameters, and additional settings associated with the deposition laser and expected build volume can be found in Table 5. The nozzles were visually inspected after deposition and no additional wear was found. The width and length of the samples were measured using a digital microscope, and bead height was measured with calipers.

3.6. Catchment efficiency calculation

Catchment efficiency was twice calculated using both the diametric ratio described in Eq. (9) and the approximate build volume of each deposition sample. For the first method, the definition of powder stream diameter was set at ± 2σ, as this is also the definition of the deposition laser spot size (equivalent to the $1/e^2$ edge definition) [35]. This was performed using traverse profiles of particle luminance at the deposition

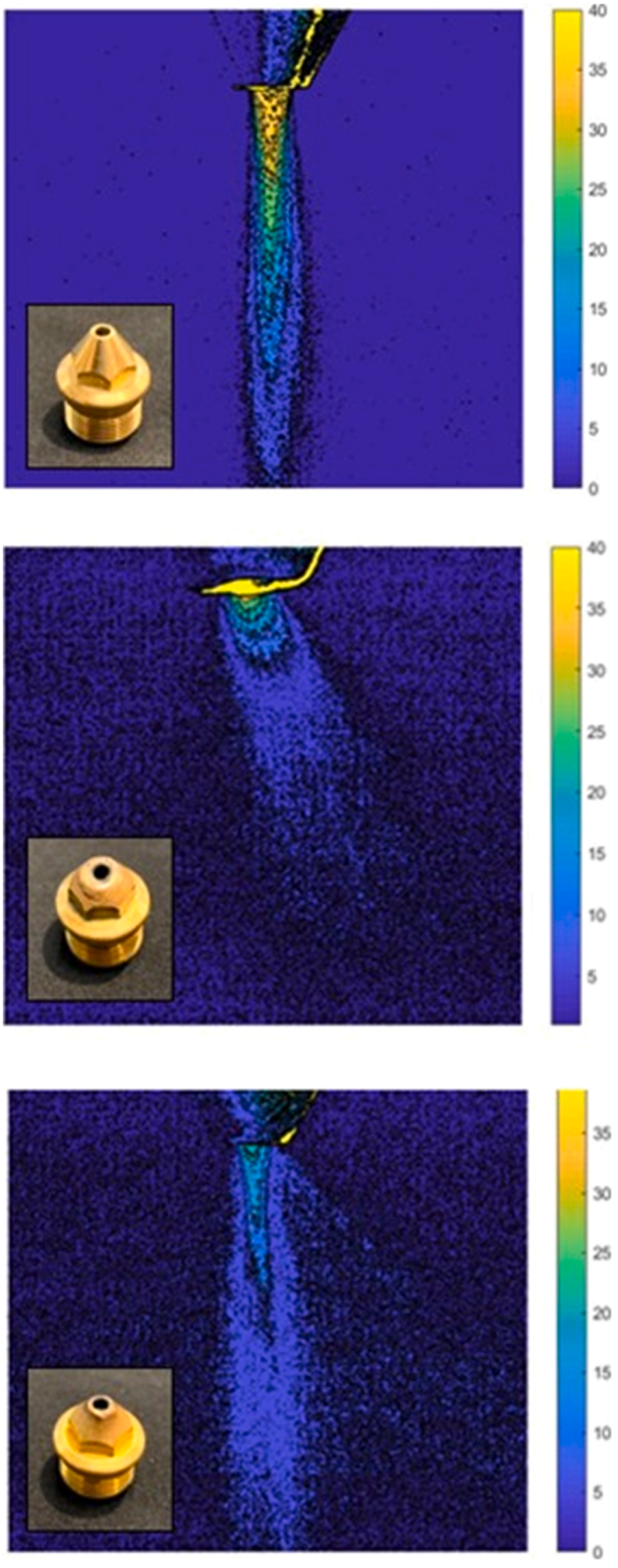

Fig. 10. Powder streams produced by a new nozzle (top), and those produced by melted (center) and abraded (bottom) nozzles.

standoff height for both experimental and simulated flows, and the spot size diameter of the deposition laser, 1.00 mm. In the second method, deposited build mass is roughly approximated by multiplying measured build volume by 8000 kg/m^3, the density of 316 L SS. This is compared to the mass of supplied powder, calculated from clad speed, clad length, and powder feed rate [36].

4. Results

Qualitative observations of powder streams from retired mid-coaxial nozzles revealed two possible sources of wear induced flow anomalies. The first of two noticed geometric irregularities related to tip wear was an altered outer contour indicative of the nozzle tip melting and resolidifying, which is more likely to occur during higher power deposition operations. The other type of geometric irregularity was a jagged, uneven nozzle tip indicative of erosion by powder abrasion. Powder streams produced by both geometric irregularities are presented in contrast to a new, off-the-shelf nozzle in Fig. 10.

The mid-coaxial nozzles produced with replicated geometry demonstrated reduced, yet similar performance compared to new, manufacturer supplied nozzles as seen in Fig. 11. Basic geometric powder stream properties were measured in both the retired nozzle and those with manufactured tip wear in order to better associate powder stream anomalies with a wear related cause. After identifying the axial distance of the consolidation plane at which powder stream waist was thinnest, a linear regression model was used to calculate the average angle of convergence and divergence in powder flow regions located above and below the consolidation plane, respectively. As retired nozzles did not have a radially symmetric surface of wear, the powder flow boundary on either nozzle side was considered a separate profile, and powder stream angles are reported in order of least to greatest wear. Powder stream angles corresponding to nozzles with manufactured wear are similarly treated, but final angle values are reported with left and right profiles differentiated. All powder stream angles are reported with their corresponding intervals of uncertainty.

In Fig. 12, a wide array of convergent and divergent powder stream angles occurred. Despite its location above the consolidation plane, the average angle of each imaged powder stream was observed to be divergent from the outer nozzle exit in nearly every case of wear greater than 0 mm at the $\pm 2\sigma$ stream edge definition. As a result, the stream was analyzed at the $\pm \sigma$ edge as well. Powder stream convergence angles at both $\pm \sigma$ and $\pm 2\sigma$ displayed divergent behavior in multiple profiles. For viewing clarity, a convergent data entry was omitted from the figure if a powder flow stream was consistently divergent from the nozzle exit to the end of the region of interest. Angle values in Fig. 13 demonstrate more of a straightening in powder flow. Even at a wider $\pm 2\sigma$ interval, convergent flow is observed in all wear states, although both convergent and divergent angles decrease with wear. Regardless, no consistent and viably measurable relationship in angle reduction, convergent or divergent, could be established. Critical dimensions of the powder consolidation plane are the standoff distance from the outer nozzle and the powder stream diameter. The retired mid-coaxial nozzles exhibited an increase in powder stream diameter with increasing wear that was constant across $\pm \sigma$ and $\pm 2\sigma$ stream edge definitions, as seen in Figs. 14 and 15 respectively. Standoff distance reflected the divergent powder flow angles calculated from the $\pm 2\sigma$ powder stream edge and noted in Fig. 12, eventually trending towards 0 mm and fully divergent flow. The inner stream edge at $\pm \sigma$ did not experience significant change in standoff distance. A general increase of minimum powder stream diameter with wear was demonstrated in both cases. In Fig. 16, one can observe that the consolidation plane dimensions in manufactured nozzles displayed a gradual linear increase in both stream diameter and standoff distance, furthering the theory that divergent outer powder streams are primarily caused by wear surfaces located on the nozzle interior.

Traverse profiles of pixel luminance and CFD simulated powder mass

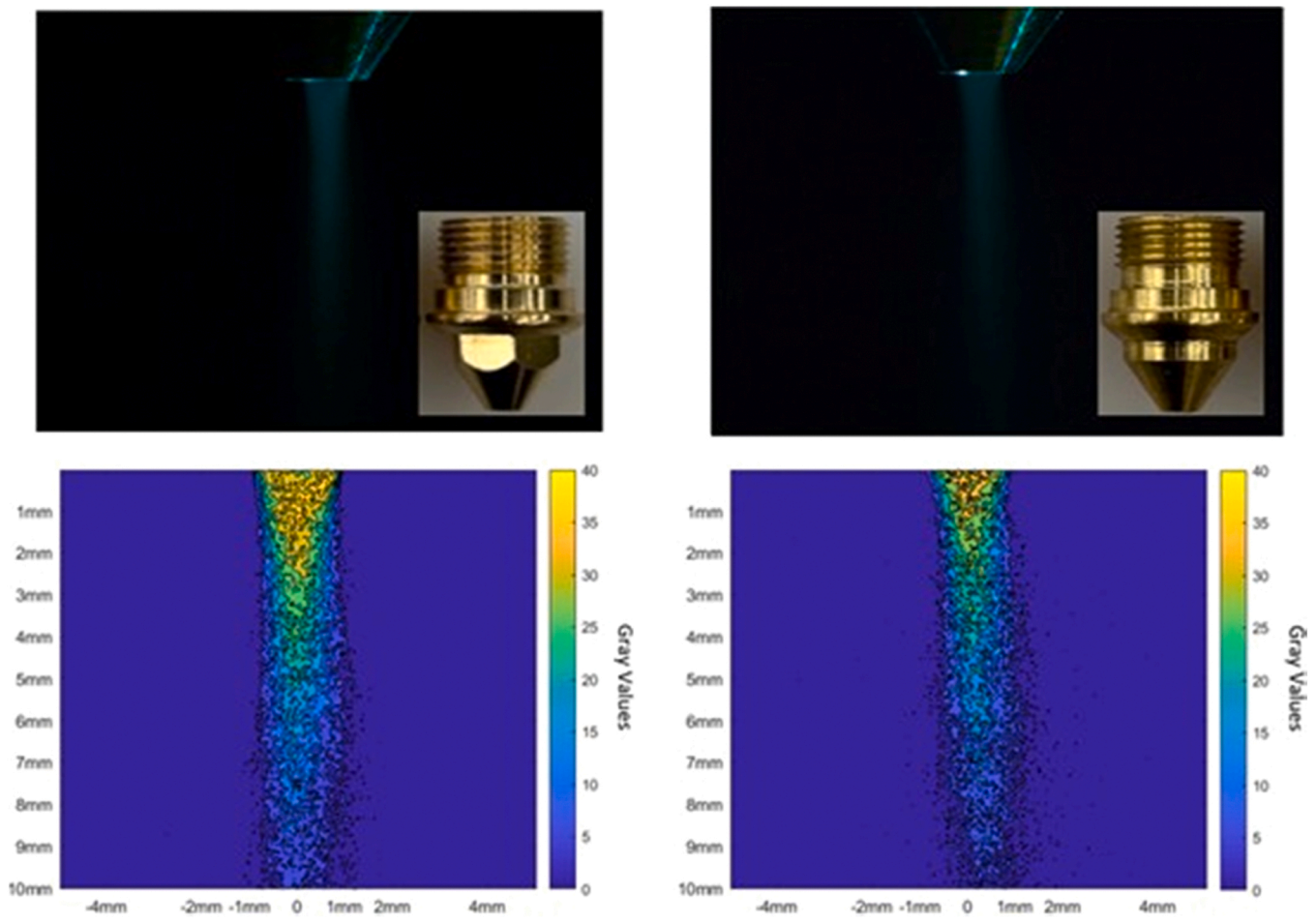

Fig. 11. Comparison of unworn nozzle flow from original (left) and replicant (right) nozzles.

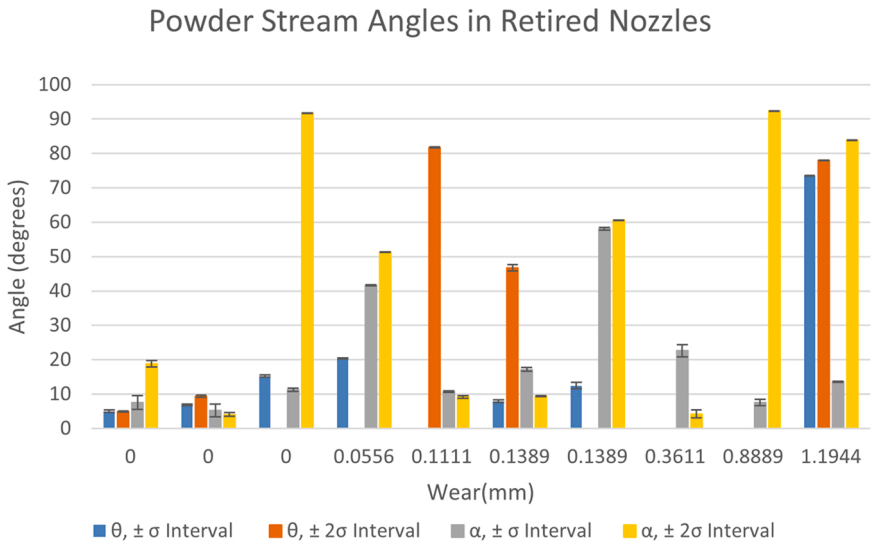

Fig. 12. Powder stream angles of convergence and divergence with wear, using nozzles retired from production. Error bars indicate the mean uncertainty of the angle's tangent, calculated using linear regression.

concentration both displayed a rough Gaussian profile centered about the coaxial cladding head center axis, despite deposition standoff distance being 1–1.75 mm above the measured plane of optimal powder stream consolidation. Powder stream characteristics obtained by CFD simulation are limited by the accuracy of initial conditions used, which were estimated from machine operating parameters rather than data acquisition. As a result, CFD simulated powder stream standard deviation ranged from 70% to 110% greater than experimental data despite trend similarity shared by both sets of data. To compare relative change in luminance and powder concentration in experimental and

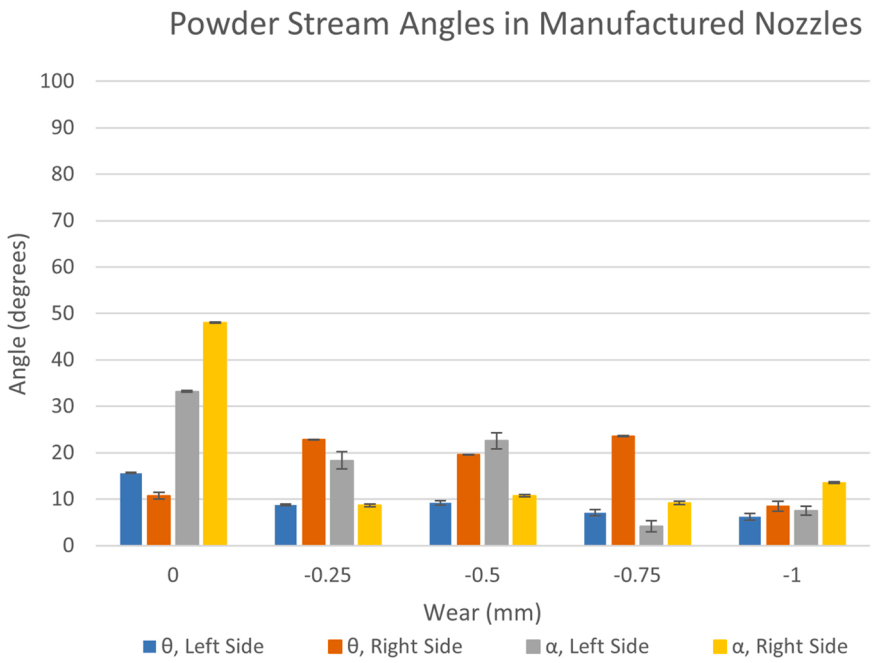

Fig. 13. Powder stream angles of convergence and divergence with wear, using nozzles with manufactured wear. Error bars indicate the mean uncertainty of the angle's tangent, calculated using linear regression.

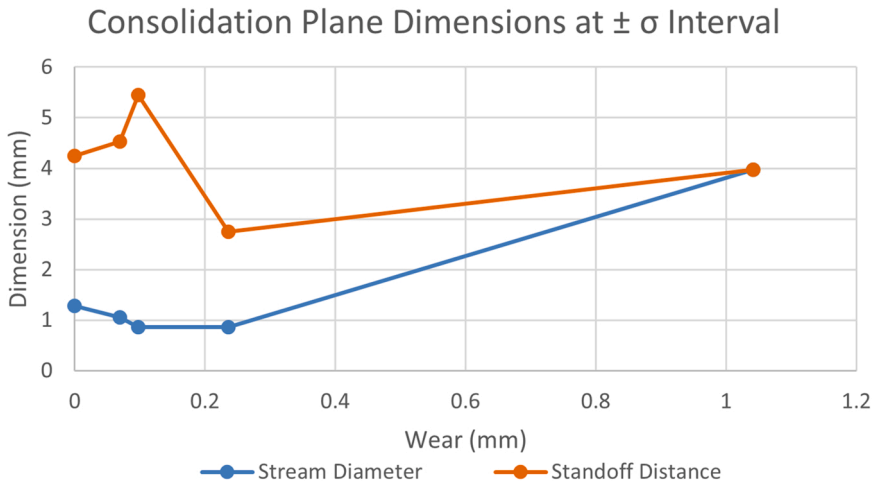

Fig. 14. Retired nozzle powder consolidation plane size and location at $\pm\sigma$ interval.

numerically simulated data respectively, both sets of data were normalized so their range is between the interval [0,1] and fitted with a first order Gaussian curve. Fig. 17 displays the normalized values as a function of their center axis offset, which was not subject to data processing methods such as normalization or scaling.

Catchment efficiency of experimental and numerically simulated data sets, along with their respective curves of best fit were calculated using Eq. (9) and compared to catchment efficiency ascertained from deposition build volume measurements listed in Table 6. The results were plotted as line graphs to show catchment efficiency loss with increasing wear in Fig. 18. Catchment efficiency from build volume was understandably lower than experimental values in all trials, as powder stream imaging does not account for any loss in catchment suffered by the presence of substrate, particularly in particles rebounding out of the melt pool. Curves of best fit had lower catchment than the data sets they represent as data distribution tended to be weighted slightly toward the center axis, or curve midpoint, rather than at its tails. While CFD simulated powder concentration was observed to be geometrically inconsistent with experimental measurements of powder stream width, corresponding catchment efficiency values fell within a reasonable interval (between deposition and experimental values), due to the weighting caused by the presence of maximum powder concentration about center axis.

In summary, all testing methods displayed a 15–20% reduction in powder catchment sustained in a roughly linear trend up to − 1.0 mm of axial tip reduction and were similar in value to catchment efficiencies mentioned in literature for laser based, powder fed DED systems.

5. Discussion

The dimensional characteristics of the consolidation plane measurements for mid-coaxial nozzles with manufactured wear trend similarly to the $\pm\sigma$ consolidation plane measurements, as opposed to the divergent behavior observed at the powder stream outer edge (retired nozzle results). This appears to indicate that the observed interior wear regions impact the edges of the powder stream the most, a region of

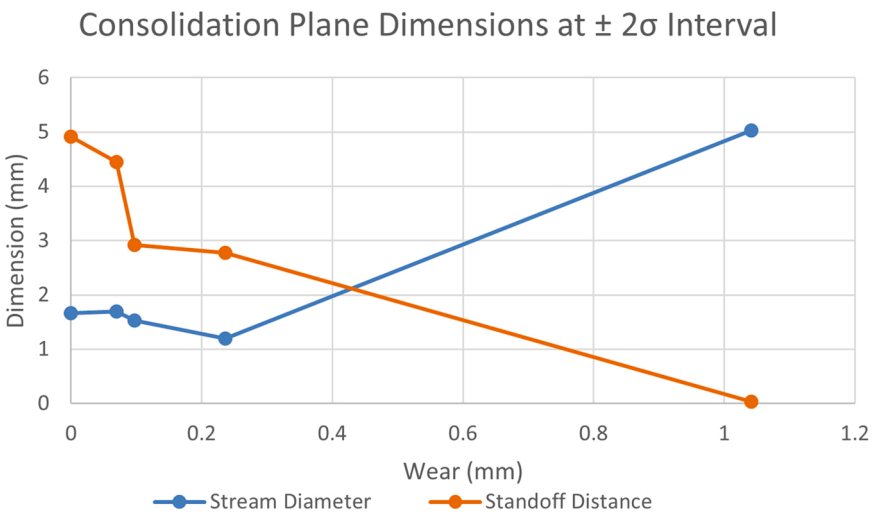

Fig. 15. Retired nozzle powder consolidation plane size and location at ± 2σ interval.

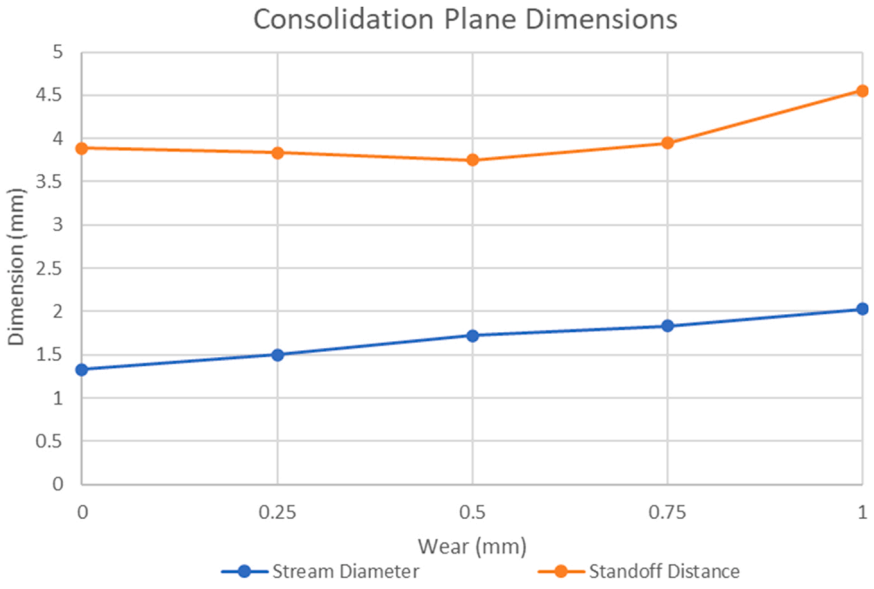

Fig. 16. Manufactured nozzle powder consolidation plane size and location (at ± 2σ interval).

decreased powder concentration. This behavior is confirmed in manufactured wear nozzle measurements, which indicated a steady linear increase in stream diameter with wear, while standoff distance has no observable linear trend. In catchment efficiency calculations, the rate of increase in stream diameter transitions to a decrease in catchment efficiency. While consolidation plane measurements are not powder catchment ratios, any increase in powder stream diameter can be assumed to cause a decrease in catchment efficiency, as the diameter of the deposition laser remained constant throughout all experiments. In contrast, a concrete relationship between catchment efficiency and standoff distance could not be established without further data collection.

Initial observations of nozzle wear types indicated that the rate of wear differs depending on deposition laser and powder flow process parameters, so monitoring nozzle wear was determined to be more prudent in maintaining constant performance, as opposed to monitoring a nozzle's overall lifetime from installation to retirement. The current methods of monitoring nozzle wear are usually visual inspection or by using a physical gage. These methods are only possible at the start or the end of a deposition operation, and they do not give insight into powder flow shape. Incorporating light sheet imaging as a method of flow calibration would allow for process parameter adjustment to best optimize powder flow geometry. In this study, light sheet image equipment was affixed to the spindle column to demonstrate the possibility of checking on nozzle health before, during, and after future deposition cycles. As the experiment design discussed in this study images a cold powder stream, mid-cycle checks could be incorporated in machine code and even coordinated with dwell times used as a thermal regulation measure.

Parameters with potential for process improvement must either alter the diameter of powder flow or the diameter of the deposition laser. As the deposition laser diameter could not be altered without incurring significant damage to the AM head assembly, parameter adjustment to improve powder catchment must change powder flow geometry in a significant way. Three parameters that fit this condition are standoff distance, shield gas flow rate, and carrier gas flow rate. While aligning the standoff distance to the consolidation plane of the mid-coaxial nozzle would not directly change powder stream geometry in any way, it would ensure that powder impacts the melt pool at its smallest diameter. Changing the standoff distance introduces a complication if

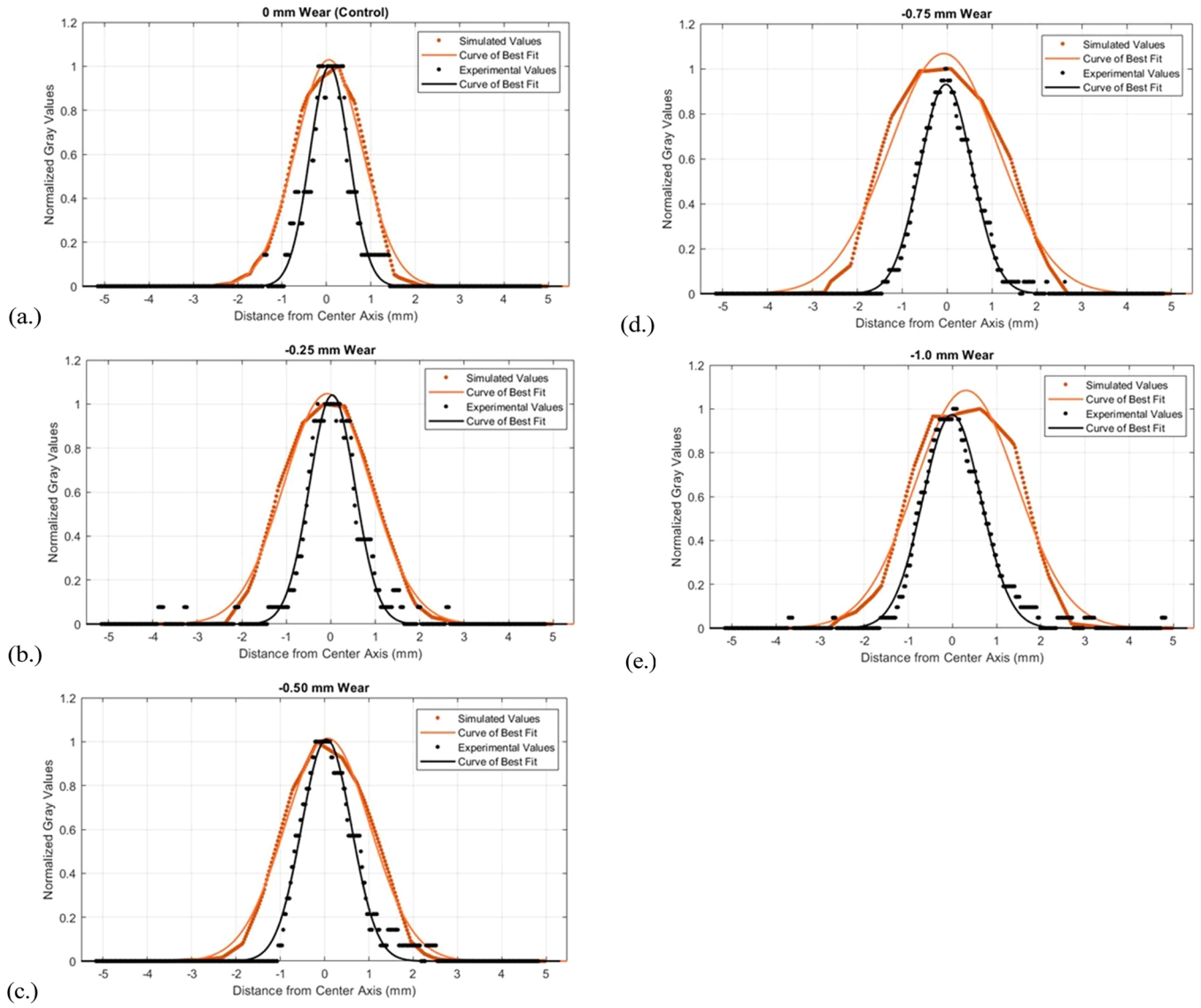

Fig. 17. Traverse profiles of experimental and CFD simulated powder flows at deposition height 2.75 mm. Profiles are listed in order of increasing wear, a) control nozzle without wear, b) −0.25 mm wear, c) −0.5 mm wear, d) −0.75 mm wear, e) −1.0 mm wear.

Table 6
Catchment efficiency calculated from single bead deposition build volume.

Trial	Average volume (mm^3)	Calculated mass (g)	Catchment efficiency
Control	8.601 ± 0.5361	6.881E-2 ± 4.2886E-3	0.6514 ± 6.451E-2
-0.25 mm Wear	8.331 ± 0.2483	6.664E-2 ± 1.986E-3	0.6309 ± 4.196E-2
-0.50 mm Wear	5.608 ± 0.3662	4.487E-2 ± 2.930E-3	0.4248 ± 4.333E-2
-0.75 mm Wear	4.498 ± 0.3021	3.598E-2 ± 2.417 E-3	0.4248 ± 4.333E-2
-1 mm Wear	4.843 ± 0.5651	3.874E-2 ± 4.521E-3	0.4248 ± 4.333E-2

the deposition laser focal distance cannot be easily adjusted to match the standoff distance, as increased laser attenuation could significantly alter the thermal gradient of the stream and melt pool [37,39,64]. Changing the carrier or shield gas flow rate throughout the life of the nozzle could also optimize catchment efficiency and may be a more apt method of adjusting parameters to alter powder spot size [26,36]. Although it would increase material usage, it would not interfere with the laser as when changing standoff distance.

Another potential benefit of powder stream parameter manipulation is the ability to prioritize certain maintenance operations. In this study, deposition height was set at 2.75 mm, the current axial offset distance of the deposition laser focal plane. The manufacturer supplied machine specifications list laser focal length at 5 mm offset from nozzle end, and while operational, the laser optics within the hybrid manufacturing machine tool need recalibration. In an industrial application, fixing or modifying nozzle geometry to match laser spot size and changing the nozzle offset may be a beneficial short-term fix so that necessary laser recalibration may occur at a time least intrusive to the workflow [65]. This is an excellent example of how predictive maintenance and monitoring of material, tooling, and machine health can determine the effectiveness of implementing ZDM. Awareness of the state of these manufacturing elements beforehand, not just detecting potential defects during the manufacturing process, can have instrumental consequences on process quality control.

Although the results of the accompanying CFD simulation were geometrically inconsistent with experimental measurements of powder stream width, the catchment efficiency of the CFD simulation was within

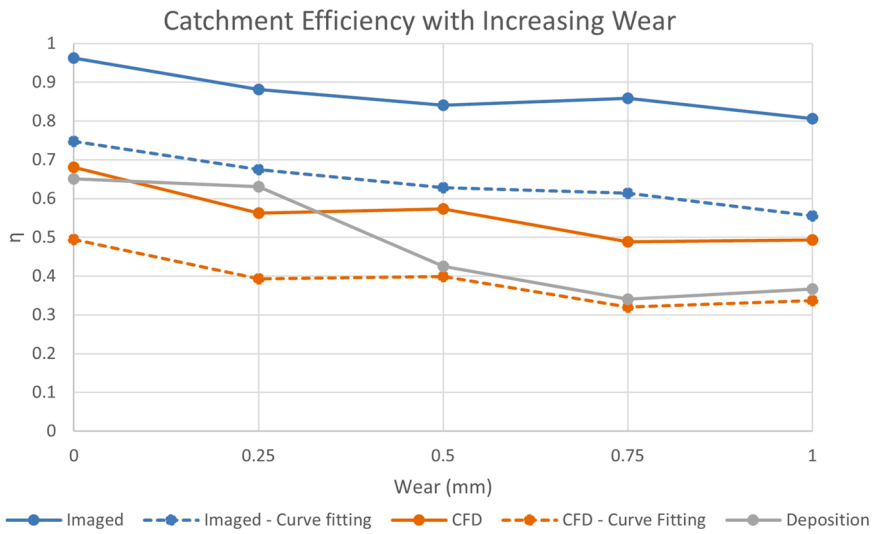

Fig. 18. Comparison of catchment efficiency calculation methods.

range of the deposition catchment efficiency, displayed the same Gaussian distribution behavior as the experimental data set, and decreased in catchment efficiency at a roughly linear rate. The low deposition catchment efficiency calculated as a mass ratio is understandable, as imaging free flowing powder does not account for complex multiphase interactions occurring as powder particles collide with melt pool. The CFD simulation can be improved by altering parameters until the traverse powder profiles closely match the experimental results, but this would limit use of the simulation to the tested parameter set, rather than predicting powder stream behavior. Regardless of the necessity for accurate numerical simulation of powder width, the developed simulation is useful in estimating powder catchment at various wear states and standoff distances, as a wider uncertainty interval can be allowed due to the location of high concentration regions of a normal Gaussian distribution. In its current state of development, following this methodology for a particular parameter set could predict powder catchment losses and prevent the running of the machine tool in a high error state. With more accurate parameter values for setting CFD simulation initial conditions, nozzle geometry could be optimized using CFD modeling to fit specific manufacturing applications, much like how custom tooling is produced for specific manufacturing applications in CNC machining centers.

6. Conclusions

This study focused on developing preliminary relationships between nozzle wear and characteristics of the resultant powder stream and deposition. These characteristics were measured using experimental and numerical flow visualization techniques, and also confirmed from a material properties perspective through deposition testing of 316 SS. The principal conclusions of this study are as follows:

1. Nozzle wear regions located on the inner contour likely affect edge regions of the resulting powder stream.
2. Axial reduction in nozzle tip is associated with an increase in powder stream diameter.
3. Standoff distance is likely affected by light to moderate amounts of axial nozzle tip wear.
4. Axial reduction in nozzle tip corresponds to a loss in build volume.
5. Catchment efficiency is negatively affected by increasing amounts of nozzle tip wear.

The first of these conclusions, the impacts of inner nozzle wear regions on powder stream geometry, was obtained by comparing the standoff distance of the consolidation plane in retired nozzles using edge definitions $\pm\sigma$ and $\pm 2\sigma$. The wider edge definition standoff distance trended toward zero with increasing wear and was observed to have a diverging flow at or near the nozzle exit. In contrast, the $\pm\sigma$ edge definition standoff distance followed a similar trend as the standoff distance calculated from nozzles with manufactured wear. As powder concentration decreases toward the edge of the powder stream, this conclusion likely contributes a small fraction of loss in catchment efficiency but a dominant effect in powder stream edge definition.

The connection between nozzle tip reduction due to wear and the measured build volume losses are associated with loss in catchment efficiency approximated by powder mass ratio. Likewise, nozzle tip reduction contributing to a widening powder stream diameter directly affects catchment efficiency approximated by a laser and powder stream diametric ratio. Both approximations of catchment efficiency decreased with the incremental increase of nozzle tip wear, and addressing this issue is critical in maintaining a near defect free manufacturing environment.

The contributions of this study lie in the adaptation of experimental methods traditionally applied to the design validation and qualification of middle coaxial nozzles into a procedure of performance monitoring that can be used throughout the lifetime of the nozzle. In doing so, types of wear exhibited by these nozzles were observed and categorized, and foundational relationships were developed between nozzle wear geometry (specifically axial tip reduction), powder stream geometry, and deposition volume. Lastly, the impact of nozzle tip wear on catchment efficiency was quantified by diametric and mass ratio approximations. This conclusion establishes foundational knowledge of a new opportunity for process optimization in powder fed, coaxial DED systems, and the ability to improve one of its most critical drawbacks.

This study's limitations stem from a variety of factors that could skew the relationships presented. As only five levels of wear were tested, this study would greatly benefit from more data points. In addition, the methods used in the catchment efficiency calculations were intended as approximations of machine performance. Equipment based limitations exist in the weld pool camera resolution, beam diameter of the line laser, and rigidity of mounts used to affix these objects to the spindle column. The most pressing limitation present in the hybrid manufacturing machine tool is an inability to ensure powder mass flow regularity during deposition. It is also worth mentioning that the deposition laser on this machine was in need of recalibration, and that the AM head nozzle geometry was likely originally optimized for a standoff distance of 5 mm. Lastly, deposition catchment could be influenced by the location of the deposited samples on the substrate. The data presented in this study

Table A.7
Powder stream angles in retired nozzles.

Wear (mm)	θ, $\pm\sigma$ Interval	θ, $\pm 2\sigma$ Interval	α, $\pm\sigma$ Interval	α, $\pm 2\sigma$ Interval
0	4.9956 ± 0.3793	4.8562 ± 0.1684	7.5310 ± 2.0600	18.8028 ± 0.9550
0	6.8317 ± 0.2153	9.4392 ± 0.2849	5.2466 ± 1.8240	4.0567 ± 0.5990
0	15.2142 ± 0.3008	–	11.2617 ± 0.4172	91.7315 ± 0.0556
0.0556	20.3448 ± 0.0891	–	41.6083 ± 0.1283	51.2774 ± 0.03778
0.1111	–	81.7384 ± 0.1925	10.7106 ± 0.2215	9.1798 ± 0.3627
0.1389	7.8887 ± 0.2483	46.7563 ± 0.9456	17.1724 ± 0.4928	9.3917 ± 0.09319
0.1389	12.4644 ± 0.9673	–	58.1060 ± 0.3981	60.6118 ± 0.05193
0.3611	–	–	22.5776 ± 1.753	4.1809 ± 1.1860
0.8889	–	–	7.4988 ± 0.9492	92.3570 ± 0.009103
1.194	73.4533 ± 0.0512	78.0141 ± 0.0995	13.5166 ± 0.1723	83.8586 ± 0.03289

Table A.8
Powder stream angles in fabricated nozzles.

Wear (mm)	θ, Left Side	α, Left Side	θ, Right Side	α, Right Side
0	15.6274 ± 0.1415	33.1766 ± 0.158	10.7363 ± 0.6926	47.9842 ± 0.1067
-0.25	8.8061 ± 0.1684	18.3380 ± 1.847	22.8408 ± 0.0471	8.6583 ± 0.3412
-0.50	9.2061 ± 0.4994	22.57756 ± 1.753	19.6008 ± 0.0431	10.7106 ± 0.2215
-0.75	7.0803 ± 0.6037	4.1808 ± 1.186	23.5668 ± 0.1014	9.1798 ± 0.3627
-1.0	6.2061 ± 0.7420	7.4987 ± 0.9492	8.4245 ± 1.0570	13.5165 ± 0.1723

should be carefully interpreted and concrete relationships between wear and component aspects of powder fed DED performance should be refrained from until a larger body of data exists.

The work presented is composed of initial findings that indicate a need for greater understanding in assessing the impact of wear in replaceable AM components on machine performance. In quantifying the effects of coaxial nozzle wear, only one of two identified geometric irregularities was thoroughly investigated, and the effects of wear on interior nozzle surfaces as well as the combined effects of both forms of wear should be studied in depth. Other areas of interest include material properties analysis of the deposited samples to determine whether a relationship exists between nozzle wear and material defects, such as pores and cracking. Once the effects of coaxial nozzle wear geometry are fully understood, the viability of adjusting relevant process parameters should be studied for potential closed loop control applications, for manufacturing sustainability optimization, and other forms of in-process monitoring and correction. In summary, this study provided a first look into new opportunities for improved performance in powder-fed AM systems and insight into the consequential effects consumables have on deposition quality. There are many openings for further work, and the total comprehension of this topic.

Declaration of Competing Interest

The authors declare that they have no known competing financial interests or personal relationships that could have appeared to influence the work reported in this paper.

Table A.9
Retired nozzle consolidation plane dimensions at $\pm\sigma$ Interval.

Average wear (mm)	Powder stream diameter (mm)	Standoff distance (mm)
0	1.2778	4.25
0.0695 ± 0.0491	1.0556	4.5278
0.0973 ± 0.0295	0.8611	5.4444
0.2361 ± 0.0884	0.8611	2.75
1.0417 ± 0.1080	3.9722	3.9722

Table A.10
Retired nozzle consolidation plane dimensions at $\pm 2\sigma$ Interval.

Average wear (mm)	Powder stream diameter (mm)	Standoff distance (mm)
0	1.6667	4.9167
0.0695 ± 0.0491	1.6944	4.4444
0.0973 ± 0.0295	1.5278	2.9167
0.2361 ± 0.0884	1.1944	2.7778
1.0417 ± 0.1080	5.0278	0.0278

Table A.11
Manufactured nozzle consolidation plane dimensions at $\pm 2\sigma$ Interval.

Average wear (mm)	Powder stream diameter (mm)	Standoff distance (mm)
0	1.3333	3.8889
-0.25	1.5000	3.8333
-0.50	1.7222	3.75
-0.75	1.8333	3.9444
-1.0	2.0278	4.5556

Table A.12
Manufactured nozzle consolidation plane dimensions at $\pm 2\sigma$ Interval.

Trial	Mean width (mm)	Mean length (mm)	Mean height (mm)
Control	1.0470 ± 0.0174	13.0604 ± 0.0635	0.6514 ± 6.451E-2
-0.25 mm Wear	1.0335 ± 0.0095	13.0857 ± 0.0564	0.6309 ± 4.196E-2
-0.50 mm Wear	0.9298 ± 0.0161	13.0276 ± 0.0268	0.4248 ± 4.333E-2
-0.75 mm Wear	0.8549 ± 0.0243	12.9582 ± 0.0381	0.3407 ± 3.538E-2
-1.0 mm Wear	0.9002 ± 0.0275	13.0264 ± 0.0635	0.3668 ± 5.626E-2

Acknowledgments

This work was supported in part by the U.S. Department of Energy through award DE-EE0008303.

Appendix A

A.1. Tabulated powder stream angle data

These tables accompany Fig. 12 and Fig. 13.
See Tables A.7 and A.8.

A.2. Tabulated consolidation plane dimensions

These tables accompany Figs. 14, 15 and 16.
See Tables A.9–A.11.

A.3. Tabulated deposition sample dimensions

This table accompanies Table 6.
See Table A.12.

References

[1] Pinkerton AJ. Laser direct metal deposition: theory and applications in manufacturing and maintenance; 2010.

[2] Dass A, Moridi A. State of the art in directed energy deposition: From additive manufacturing to materials design. Coatings 2019;9:418.
[3] Bourell D, Kruth J-P, Leu M, Levy G, Rosen D, Beese A, et al. Materials for additive manufacturing. CIRP Ann Manuf Technol 2017;66(06).
[4] Lin J, Steen WM. Design characteristics and development of a nozzle for coaxial laser cladding. J Laser Appl 1998;10:55–63.
[5] Yamazaki T. Development of a hybrid multi-tasking machine tool: Integration of additive manufacturing technology with cnc machining. Procedia CIRP 2016;42:81–6.
[6] Kovaleva I, Kovalev O, Zaitsev AV, Sergachev DV. Modeling and numerical study of light-propulsion phenomena of particles acceleration in coaxial laser powder cladding. Phys Procedia 2014;56:439–49.
[7] Baumers M, Dickens P, Tuck C, Hague R. The cost of additive manufacturing: Machine productivity, economies of scale and technology-push. Technol Forecast Soc Change 2016;102:193–201.
[8] Zhong ZY, Kai SL, Fēng Xj, Xīn ZX, Jùn X. Laser coating coaxial powder-delivery nozzle. China Patent CN2510502Y; 2003.
[9] Qiáng YY, Yǒng H. Ring type coaxial laser cladding nozzle. China Patent CN2707772Y; 2005.
[10] Krause A, Uelze A, Becker R. Ring type coaxial laser cladding nozzle. United States Patent US005321228A; 1994.
[11] Buongiorno A. Laser/powdered metal cladding nozzle. European Patent EP0741626B1; 2002.
[12] Guo W. Compact coaxial nozzle for laser cladding. United States Patent US20060065650A1; 2006.
[13] Hu Y. Coaxial nozzle design for laser cladding/welding process. United States Patent US20050056628A1; 2005.
[14] Lowney MTJ. Nozzle particularly suited to direct metal deposition. United States Patent US006534745B1; 2003.
[15] Freneaux O, Poulet JB, Lepre O, Montavon G. Coaxial nozzle for surface treatment by laser irradiation, with supply of materials in powder form. United States Patent US005418350A; 1995.
[16] Yang L, Hsu K, Baughman B, Godfrey D, Medina F, Menon M, Wiener S. Additive manufacturing of metals: the technology, materials, design and production; 2017.
[17] Wohlers TT, Caffrey T. Wohlers report 2013: additive manufacturing and 3d printing state of the industry: annual worldwide progress report; 2013.
[18] Niaki K. The management of additive manufacturing; 2018.
[19] Bourhis FL, Kerbrat O, Dembinski L, Hascoët J-Y, Mognol P. Predictive model for environmental assessment in additive manufacturing process. Procedia CIRP 2014;15:26–31.
[20] LLC S, Association AMGT, Inc TE. Overview of disposal procedures for powder condensate within metal powder bed fusion; 2021.
[21] Lorenz KA. A review of hybrid manufacturing. In: Proceedings of the 26th annual international solid freeform fabrication symposium; 2015. p. 96–108.
[22] Kim FH, Moylan SP. Advanced manufacturing series 10016 literature review of metal additive manufacturing defects; 2018.
[23] Hu D, Kovacevic R. Sensing, modeling and control for laser-based additive manufacturing. Int J Mach Tools Manuf 2003;43:51–60.
[24] McLean M, Shannon GJ, Steen WM. Laser generating metallic components. In: Proceedings of the XI international symposium on gas flow and chemical lasers and high-power laser conference; 1997.
[25] Resch M, Kaplan AFH, Schuoecker D. Laser-assisted generating of three-dimensional parts by the blown powder process. In: Proceedings of the XIII international symposium on gas flow and chemical lasers and high-power laser conference; 2001.
[26] Takemura S, Koike R, Kakinuma Y, Sato Y, Oda Y. Design of powder nozzle for high resource efficiency in directed energy deposition based on computational fluid dynamics simulation. Int J Adv Manuf Technol 2019;105:4107–21.
[27] DeWitte LN, Saldana CJ, Feldhausen TA, Kurfess T. Initial process planning of a hybrid multi-tasking platform. In: Proceedings of the ASME 2020 15th international manufacturing science and engineering; 2020.
[28] HernándezKorner M, Lambán M, Albajez J, Santolaria J, NgCorrales LDC, Royo J. Systematic literature review: Integration of additive manufacturing and industry 4.0. Metals 2020;10:1061.
[29] Ahuett-Garza H, Kurfess T. A brief discussion on the trends of habilitating technologies for industry 4.0 and smart manufacturing. Manuf Lett 2018;15:60–3.
[30] Psarommatis F, May G, Dreyfus P-A, Kiritsis D. Zero defect manufacturing: state-of-the-art review, shortcomings and future directions in research. Int J Prod Res 2019;58:1–17. https://doi.org/10.1080/00207543.2019.1605228.
[31] Psarommatis F, Sousa J, Mendonçab JP, Mendonça DK. Zero-defect manufacturing the approach for higher manufacturing sustainability in the era of industry 4.0: a position paper. Int J Prod Res 2021.
[32] Jones JB. The synergies of hybridizing cnc and additive manufacturing; 2016.
[33] Coates P, Jones JB. Material processing methods and related apparatus. United States Patent US20170129180A1; 2017.
[34] Coates P, Jones JB. Apparatus for workpiece processing having integrated energy guide and media storage and related system and method. United States Patent US009586298B2; 2017.
[35] Marshall GF. Handbook of optical and laser scanning. 2004.
[36] Lin J. Simple model of powder catchment in coaxial laser cladding. Opt Laser Technol 1999;31:233–8.
[37] Lin J. Laser attenuation of the focused powder streams in coaxial laser cladding. J Laser Appl 2000;12:28–33.
[38] Pinkerton AJ, Lin L. Modelling powder concentration distribution from a coaxial deposition nozzle for laser-based rapid tooling. J Manuf Sci 2004;126:33–41.
[39] Pinkerton AJ. An analytical model of beam attenuation and powder heating during coaxial laser direct metal deposition. J Phys D Appl Phys 2007;40:7323–34.
[40] Pinkerton AJ, Li L. A verified model of the behaviour of the axial powder stream concentration from a coaxial laser cladding nozzle. In: Proceedings of the 21st international congress on applications of lasers and electro-optics; 2014. p. 75–174.
[41] Guan X, Zhao YF. Numerical modeling of coaxial powder stream in laser-powder-based directed energy deposition process. Addit Manuf 2019;34:101226.
[42] Nolan T, Lian Y, Sussman M. Development of simulation tools for selective laser melting additive manufacturing. In: Proceedings of the 28th annual international solid freeform fabrication symposium – an additive manufacturing conference; 2017. p. 1220–34.
[43] Kheloufi K, Amara EH. Numerical modelling of gas/particles diphasic jet in laser cladding by coaxial nozzle. Phys Procedia 2010;5:347–52.
[44] Zhang B, Coddet C. Numerical study on the effect of pressure and nozzle dimension on particle distribution and velocity in laser cladding under vacuum base on cfd. J Manuf Process 2016;23:54–60.
[45] Tabernero I, Lamikiz A, Ukar E, López De Lacalle LN, Angulo C, Urbikain G. Numerical simulation and experimental validation of powder flux distribution in coaxial laser cladding. J Mater Process Technol 2010;210:2125–34.
[46] ANSYS I. Ansys fluent theory guide; 2013.
[47] Morsi SA, Alexander AJ. An investigation of particle trajectories in two-phase flow systems. J Fluid Mech 1972;55:193–208.
[48] Everton SK, Hirsch M, Stavroulakis PI, Leach RK, Clare AT. Review of in-situ process monitoring and in-situ metrology for metal additive manufacturing. Mater Des 2016;95:431–45.
[49] Marshall GJ, Thompson SM, Shamsaei N. Data indicating temperature response of ti-6al-4v thin-walled structure during its additive manufacture via laser engineered net shaping. Data Brief 2016;7:697–703.
[50] Griffith ML, Schlienger ME, Harwell LD, Oliver M, Baldwin MD, Ensz MT, et al. Understanding thermal behavior in the lens process. Mater Des 1999;20:107–13.
[51] Yu J, Lin X, Wang J, Chen J, Huang W. Mechanics and energy analysis on molten pool spreading during laser solid forming. Appl Surf Sci 2010;256:4612–20.
[52] Nassar AR, Keist J, Reutzel EW, Spurgeon TJ. Intra-layer closed-loop control of build plan during directed energy additive manufacturing of ti-6al-4v. Addit Manuf 2015;6:39–52.
[53] Wang L, Felicelli S, Craig J. Thermal modeling and experimental validation in the lenstm process. In: Proceedings of the 18th solid freeform fabrication symposium, SFF; 2007, 012007.
[54] Hua T, Jing C, Xin L, Fengying Z, Weidong H. Research on molten pool temperature in the process of laser rapid forming. J Mater Process Technol 2008;198:454–62.
[55] Tan H, Fang Y, Zhong C, Yuan Z, Wei F, Li Z, et al. Investigation of heating behavior of laser beam on powder stream in directed energy deposition. Surf Coat Technol 2020;397:126061.
[56] Ibarra-Medina J, Pinkerton AJ. A cfd model of the laser, coaxial powder stream and substrate interaction in laser cladding. Phys Procedia 2010;5:337–46.
[57] Ibarra-Medina J, Vogel M, Pinkerton AJ. A CFD model of laser cladding: From deposition head to melt pool dynamics.
[58] Tabernero I, Lamikiz A, Martínez S, Ukar E, De Lacalle LNL. Geometric modelling of added layers by coaxial laser cladding. Phys Procedia 2012;39:913–20.
[59] Liu S, Zhang Y, Kovacevic R. Numerical simulation and experimental study of powder flow distribution in high power direct diode laser cladding process. Lasers Manuf Mater Process 2015;2:199–218.
[60] Balu P, Leggett P, Kovacevic R. Parametric study on a coaxial multi-material powder flow in laser-based powder deposition process. J Mater Process Technol 2012;212:1598–610.
[61] Van De Hulst HC. Light scattering by small particles; 1957.
[62] New mazak vc-500 am combines 5-axis and additive technology to revolutionize product design Yamazaki Mazak Corporation; 2016. ⟨https://mazakusa.com/⟩.
[63] Kim MJ, Saldana C. Thin wall deposition of in625 using directed energy deposition. J Manuf Process 2020;56:1366–73.
[64] Kersten S, Praniewicz M, Kurfess T, Saldana C. Build orientation effects on mechanical properties of 316ss components produced by directed energy deposition. Procedia Manuf 2020;48:730–6.
[65] Gibson I, Rosen DW, Stucker B. Additive manufacturing technologies: rapid prototyping to direct digital manufacturing; 2010.